# Polarization-Sensitive Two-Photon Microscopy Study of the Organization of Liquid-Crystalline DNA

Halina Mojzisova,[†‡*] Joanna Olesiak,[§] Marcin Zielinski,[†] Katarzyna Matczyszyn,[§] Dominique Chauvat,[†] and Joseph Zyss[†]

[†]Laboratoire de Photonique Quantique et Moléculaire, and [‡]Laboratoire de Biotechnologies et de Pharmacologie Appliquée, Institut d'Alembert, Ecole Normale Supérieure de Cachan, Cachan, France; and [§]Group of Physics and Chemistry of Molecular Materials, Institute of Physical and Theoretical Chemistry, Wroclaw University of Technology, Wroclaw, Poland

ABSTRACT Highly concentrated DNA solutions exhibit self-ordering properties such as the generation of liquid-crystalline phases. Such organized domains may play an important role in the global chromatin topology but can also be used as a simple model for the study of more complex 3D DNA structures. In this work, using polarized two-photon fluorescence microscopy, we report on the orientation of DNA molecules in liquid-crystalline phases. For this purpose, we analyze the signal emitted by fluorophores that are noncovalently bound to DNA strands. In nonlinear processes, excitation occurs exclusively in the focal volume, which offers advantages such as the reduction of photobleaching of out-of-focus molecules and intrinsic 3D sectioning capability. Propidium iodide and Hoechst, two fluorophores with different DNA binding modes, have been considered. Polarimetric measurements show that the dyes follow the alignment with respect to the DNA strands and allow the determination of the angles between the emission dipoles and the longitudinal axis of the DNA double strand. These results provide a useful starting point toward the application of two-photon polarimetry techniques to determine the local orientation of condensed DNA in physiological conditions.

## INTRODUCTION

In living systems, DNA molecules are tightly packed in micrometric cell compartments. The condensation factor is very high, and DNA local concentration may reach values up to several hundreds of mg/mL (1,2). In such conditions, to decrease the entropy, the intermolecular volume is diminished by setting up a supramolecular order (3). The creation of organized structures such as liquid-crystalline domains was indeed observed in concentrated DNA (4), in both nucleosome particles and plasmid solutions, and in dinoflagellate chromosomes (5,6). These self-ordering properties are of considerable interest, because they might be related to the complex 3D chromatin topology known to influence the transcription and regulation processes in the cell nucleus (7).

The analysis of DNA liquid-crystalline domains represents the first step toward the investigation of DNA condensed states and the DNA topology in vivo. The creation of specific DNA liquid-crystalline phases gives rise to structures presenting long-term order in at least one direction. It occurs at specific temperature and concentration conditions. In simplified in vitro systems, these conditions can be achieved by increasing DNA concentration to a sufficient level. Depending on the characteristics of DNA molecules, the values of critical concentrations for the transition between the isotropic and anisotropic phases are also governed by temperature, ionic strength of the solution, and number and nature of DNA basepairs (1,8,9).

The organization of liquid-crystalline domains is mainly studied by polarized light microscopy, differential scanning calorimetry, nuclear magnetic resonance, and x-ray or electron microscopy techniques (1,8,10). These methods have brought a wealth of information about DNA liquid-crystalline phases, but they are difficult to apply to three-dimensional investigations of micrometer-thick samples in a nondestructive manner. Conversely, laser scanning microscopy techniques, such as confocal or multiphoton microscopy, are known to be well adapted to this type of study (11,12). In the latter case, the infrared pulsed excitation occurs efficiently only in the focal volume, whereas the sample or the laser beam is translated in three directions to allow a ''point-by-point'' 3D scanning. Moreover this local excitation permits minimization of the photobleaching of out-of-focus molecules. The potential of this technique can be enhanced by polarimetric analysis of two-photon processes, as was shown recently in the investigation of nonlinear properties of isolated nanoparticles (13–16).

In this work, we propose to investigate the ordering of DNA by means of polarization-sensitive two-photon microscopy. By analyzing the fluorescence emitted by fluorophores associated to DNA, we show that it is possible to extract the binding angles between the emission dipoles of these molecules and the longitudinal axis of the DNA double strands at the scale of the focal volume. We choose to work with well known DNA markers, i.e., an intercalator—propidium iodide (PI)—and Hoechst dye, which binds to the AT-rich regions in the minor groove of the DNA double helix (17,18). Comparing two dyes with different orientations relative to the DNA axis allows us to evidence the ability of

*Submitted January 29, 2009, and accepted for publication July 8, 2009.*

*Correspondence: halinam@gmail.com

Editor: Jonathan B. Chaires.



0006-3495/09/10/2348/10 $2.00

doi: 10.1016/j.bpj.2009.07.053

polarimetric analysis to distinguish between two binding modes. In the first step, we evaluate to which extent these dyes follow the DNA organization. In the next step, by adjusting the simulated theoretical data to the experimental curves, we extract the binding angles. Once the binding parameters are established, it becomes possible to infer the DNA ordering properties in liquid-crystalline phases in micrometric domains with high lateral and axial resolution.

## MATERIALS AND METHODS

### Theory

The two-photon excited volume associated to a highly focused infrared beam is of the order of a micrometer cube. Therefore a lot of dye molecules bound to DNA are excited and detected within the acquisition time. To simulate this ensemble of molecules, a simplified model was used (Fig. 1).

For each fluorophore, the emission dipole $\vec{\mu}_{em}$ forms a random azimuthal angle $\psi$ with respect to the main molecular axis of the DNA double strand. When averaging this orientation by rotating $\vec{\mu}_{em}$ by 360° around the DNA molecule, the ensemble of dipoles is uniformly spread over a "cone" of opening angle $\psi$. Variations of $\psi$ following small deviations of the DNA strand are taken into account by thickening this cone by an angular variable $\Delta\psi$.

Theoretical calculations are based on the model developed by Le Floc'h and co-workers (13,19). The macroscopic $xy$ coordinates correspond to the plane of the sample, whereas the $z$ axis is along the optical axis of the microscope, perpendicular to the sample. Rotation of the sample around the $z$ axis in the macroscopic $xy$ plane is parameterized by the angle $\phi$.

For each molecule, the measured fluorescence intensity, $I_{TPFE}$, is proportional to the probability of two-photon excitation, $P_{abs}$, combined with the emission of the fluorescence photon along the direction of the detection, $P_{em}$

$$I_{TPFE} \propto P_{abs}\, P_{em} \propto |\vec{\mu}_{abs} \times \vec{E}|^4\, |\vec{\mu}_{em} \times \vec{u}_I|^2, \qquad (1)$$

where $\vec{\mu}_{abs}$ and $\vec{\mu}_{em}$ correspond to the absorption and emission dipoles, respectively, $\vec{u}_I$ is the detection polarization, and $\vec{E}$ is the incident field at optical frequency $\omega$. To capture the large number of molecules within the excited volume, this expression has to be integrated over a conical orientation distribution of $\vec{\mu}_{abs}(\Omega)$ and $\vec{\mu}_{em}(\Omega)$, where $\Omega$ is the solid angle, leading to

$$I_I^{TPFE}(\alpha) \propto \int |\vec{\mu}_{abs}(\Omega) \times \vec{E}(\alpha)|^4\, |\vec{\mu}_{em}(\Omega) \times \vec{u}_I|^2 d\Omega. \qquad (2)$$

The polarization of $\vec{E}(\alpha)$ at the focal point is obtained through reflection of the incident laser beam on a dichroic mirror (DM) and can be varied. Therefore it is modeled as

$$\vec{E}(\alpha,\delta,\varepsilon,t) = \frac{E}{\left(1+(1-\delta)^2\right)^{1/2}} \begin{bmatrix} \cos\alpha\cos(\omega t) \\ (1-\delta)\sin\alpha\cos(\omega t+\varepsilon) \\ 0 \end{bmatrix}, \qquad (3)$$

where $E$ is the amplitude of the incident field, with $\alpha$ defining the incident polarization angle in the $xy$ reference frame, as illustrated in Fig. 2 *b*. $\delta$ and $\varepsilon$ are two parameters that account for variation of the electric field by polarization mixing and depolarization effects caused by the setup, mainly due to dichroism and birefringence properties of the DM. $\delta$ represents the ratio of the reflectivity, $r_p/r_s$, of the DM for p ($r_p$) and s ($r_s$) components, and $\varepsilon$ is the ellipticity induced by the reflection on the DM. This deformation of the initially linear polarization is schematized by the dotted ellipse in Fig. 2 *b*. The fluorescence intensities of the s ($I_x$) and p ($I_y$) polarization components are maximal for the direction of the incident electric field corresponding to $\vec{\mu}_{abs}$, assumed here to be parallel to $\vec{\mu}_{em}$. As an example, we took $\vec{\mu}_{em}$ at 45° from the $x$ axis in Fig. 2 *c*.

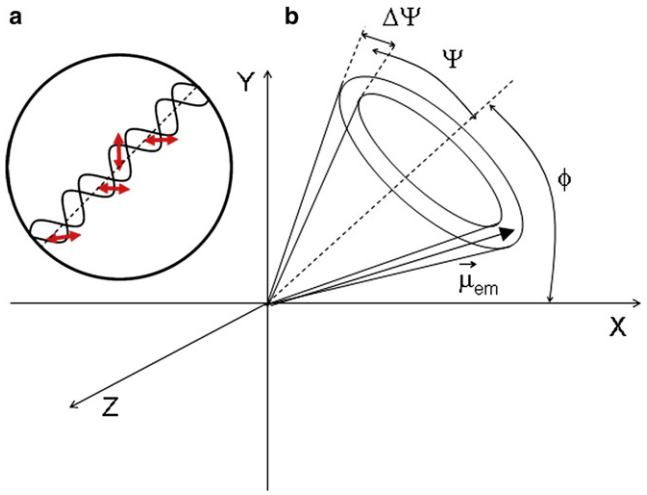


FIGURE 1 (*a*) Simplified model of the binding of an ensemble of molecules to the DNA double strand. (*b*) The emission dipoles, $\vec{\mu}_{em}$, of the dyes follow a conical distribution of a half-angle $\Psi$ with its axis along the DNA molecule. The cone has a variable thickness $\Delta\Psi$. The rotation of the DNA strand in the macroscopic framework $xy$ is accounted for by angle $\phi$.

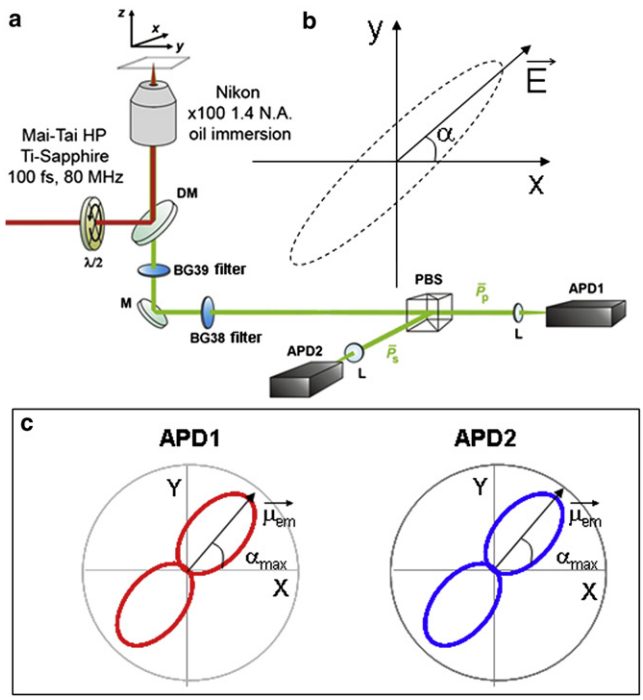


FIGURE 2 (*a*) Scheme of the experimental setup. *DM*, dichroic mirror; *M*, mirror; *PBS*, polarizing beam splitter; *APD*, avalanche photodiode; *L*, lens; *BG39* and *BG38*, filters; $\lambda/2$, half-wave plate. (*b*) For the polarimetry measurement, the incident polarization is rotated by $\alpha$ = 0–360°. In the example presented, $\alpha$ =45°. (*c*) In an anisotropic material, the $x$ and $y$ polarization components of the two-photon fluorescence intensity are measured by two avalanche photodiodes, APD1 and APD2, respectively. $\alpha_{max}$ occurs in the direction parallel to the orientation of the emitting dipoles $\vec{\mu}_{em}$. In the illustrated example, $\alpha_{max}$ = 45°.

The aim of our approach is twofold: 1), with a given orientation of DNA strands, to verify that the angle dependence of the two-photon fluorescence emitted by the dyes fixed to DNA follows our model and subsequent pattern (Figs. 1 and 2) and to determine the binding parameters $\Psi$ and $\Delta\Psi$ for PI and Hoechst; and 2), based on this calibration step, to analyze a priori unknown orientations of DNA strands in various liquid-crystalline domains.

## DNA preparation

Salmon DNA was purchased from Sigma-Aldrich (St. Louis, MO). The melting temperature is ~87.5°C. Electrophoresis on agarose gels has revealed a heterogeneous length distribution varying between 260 basepairs (bp) and 6000 bp. The main length of DNA strands is ~2000 bp. The DNA was solubilized in distilled and deionized sterile water for at least 5 h. PI and Hoechst 33342 were purchased from Molecular Probes (Eugene, OR) and the stock solutions were prepared in pure water.

Two kinds of sample were prepared: closed cells and drying droplets. In closed cells, the labeled DNA was solubilized at a concentration of 60 mg/mL. The final concentrations of PI and Hoechst were 0.30 mM and 0.16 mM, respectively, which corresponds to 1 PI molecule/320 bp and 1 Hoechst molecule/600 bp. A 50-$\mu$L sample of DNA-dye solution was deposited on a coverslip and covered by another coverslip. The spacer was made from a thin parafilm frame. The samples dried for several hours at room temperature.

For the drying droplet preparation, the DNA concentration was 5 mg/mL. The final dye concentrations were 0.81 mM and 0.67 mM for PI and Hoechst, respectively, which corresponds to 1 PI molecule/10 bp and 1 Hoechst molecule/12 bp. 15 $\mu$L of each DNA-dye solution was deposited atop a cleaned coverslip.

In all samples, the presence of liquid-crystalline domains was monitored by polarized light microscopy (PLM), e.g., observation of DNA in white light through crossed polarizers sandwiching the sample.

## Two-photon fluorescence microscopy

The scheme of the experimental setup is shown in Fig. 2 *a*. Two-photon microscopy was performed on a Nikon TE 2000-0 ECLIPSE inverted microscope. The excitation is provided by a mode-locked Ti:Sapphire laser (Mai-Tai HP, Spectra Physics, Mountain View, CA) delivering 100-fs pulses with 80-MHz repetition rate. The fundamental wavelength can be tuned from 690 to 1020 nm. The beam is focused on the sample by a high-numerical-aperture Nikon Plan Apo (100×/1.4 NA) oil immersion objective. The lateral and axial spatial resolutions are of the order of 350 and 800 nm, respectively. The signal is collected in epiconfiguration. After passing through the dichroic mirror, the $x(y)$ polarization component that coincides with the $s(p)$ incident polarization on the dichroic mirror is reflected (transmitted) by a polarizing beam-splitter, and the intensity $I_x$ ($I_y$) is detected separately by an avalanche photodiode (SPCM-AQR-14-FC, Perkin Elmer, Wellesley, MA) working in photon-counting regime. The polarization analysis is performed by recording $I_x$ and $I_y$ simultaneously while rotating the polarization of the incident light from 0° to 360° with a rotating half-wave plate ($\lambda/2$).

One important parameter of the DM is its birefringence, which leads to an ellipticity of the reflected field, accounted for by $\varepsilon$ in Eq. 3. Moreover, the multilayer coating on the DM induces a large spectral variation of this ellipticity.

The ellipsometry measurements were performed by an ellipsometer (GESP5, Sopra, Paris, France) illuminated by a white lamp in a configuration where the incidence beam impinges at 45° to the DM surface, as in the microscope.

# RESULTS

## Polarized light microscopy

As described previously (4,20), DNA in aqueous solution forms multiple lyotropic liquid-crystalline phases (LLC) that can be distinguished at a preliminary level by PLM. Similarly, DNA doped with dye molecules exhibits LLC behavior (21). LLC phases can be observed either in closed LC cells or in drying droplets. These two methods of sample preparation yield different structures at room temperature.

As shown in Fig. 3, *a* and *b*, the closed LC cells filled with solutions of DNA-PI and DNA-Hoechst present PLM images with birefringent phases where DNA strands are aligned in one direction. However, they do not form higher-order structures characteristic of cholesteric and columnar phases. These observations are in agreement with published data concerning the concentration dependence of the creation of anisotropic DNA phases (8).

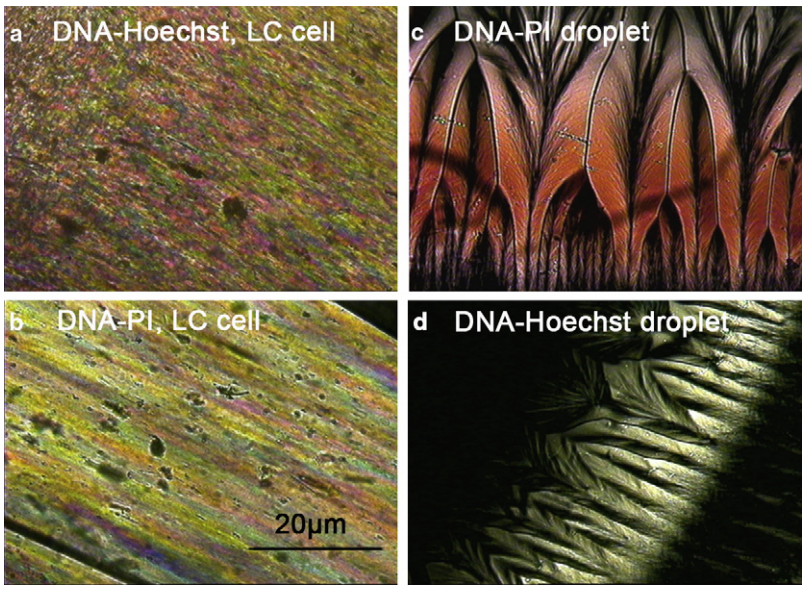


FIGURE 3 PLM images of samples. (*a*) LC cell with DNA, $c_{DNA} = 60$ mg/ml, and PI, $c_{PI} = 0.3$ mM. (*b*) Droplets of DNA, $c_{DNA} = 5$ mg/ml, and PI, $c_{PI} = 0.806$ mM. (*c*) LC cell with DNAxs, $c_{DNA} = 60$ mg/ml, and Hoechst, $c_H = 0.16$ mM. (*d*) Droplets of DNA, $c_{DNA} = 5$ mg/ml, and Hoechst, $c_H = 0.67$ mM.

PLM images of DNA-PI and DNA-Hoechst solutions with $c_{DNA} = 5$ mg/mL deposited as droplets are shown in Fig. 3, *c* and *d*. Similar characteristic zig-zag patterns were reported previously by Smalyukh et al. (22) near the rim of the droplet. They correspond to a columnar hexagonal phase with undulations induced by linear defects. In the drying process, DNA chains are deposited along the contact line. Simultaneously, they undulate due to radial stress and form striped domains that are perpendicular to the droplet boundary. Depending on the size of the droplet and the presence of local impurities on the surface of the glass, and probably on the length heterogeneity of DNA strands, different domains are formed. The width of these domains is in the range 5–30 $\mu$m for DNA-PI and 4–15 $\mu$m for DNA-Hoechst. If the domain thickness is sufficiently high, they become colorful in PLM. DNA strands within one domain are parallel, but they are bent at the border between two domains and form a specific angle with respect to the chains in the adjacent domain. The precise parameters of this structure were evaluated using two-photon microscopy.

## Two-photon microscopy

Fig. 4 shows two-photon fluorescence intensity images obtained by scanning the sample together with the corresponding polarization analysis in polar coordinates, which depicts fluorescence intensities $I_x$ and $I_y$ as a function of the incident polarization angle, $\alpha$. The two-photon fluorescence is emitted by DNA-bound PI and Hoechst. Excitation wavelengths are 920 nm and 810 nm for PI and Hoechst, respectively, and the corresponding maximum average intensities of the incident light are 1 mW and 0.5 mW. These excitation conditions were found experimentally to be the best trade-off between the photostability of the dyes and a sufficient signal/noise ratio. Under such conditions, the intrinsic fluorescence signal of pure DNA is within the noise level, thus below the detection threshold.

In the first step of evaluating the two-photon polarimetry method, we consider an isotropic DNA-PI solution. The fluorescence intensity scan of the DNA-PI solution obtained before the droplet has dried on the glass plate is shown in Fig. 4 *a*. The fluorescence scan is homogeneous. The polar graph (Fig. 4 *b*) shows a characteristic cross pattern for *x* and *y* polarization components, corresponding to random orientation of emitting dipoles. One might have expected a circle-shaped polarization response for each polarization component, in agreement with isotropically oriented dipoles. However, the preferred excitation of the dyes oriented along the polarization axis of the incident light and the detection along *x* and *y* polarization axes lead to a photoselection, well known in fluorescence polarization anisotropy experiments. Indeed, when the incident polarization is rotated by 360° in the *xy* plane and the fluorophore distribution is isotropic, the higher fluorescence intensities along *x* and *y* reflect only the separation of the emitted light by a polarizing beam-splitter along the *x* and *y* components.

In contrast, Fig. 4, *c* and *e*, displays the scanned images of liquid-crystalline domains, where PI- and Hoechst-labeled DNA double strands are aligned along the *y* direction ($\phi = 90°$). The angles of maximum fluorescence intensity in the polar graphs detected along *x* and *y* polarization axes ($I_x$ and $I_y$) are aligned along the same direction, which clearly indicates the orientation of the emitters. According to these data, it can be roughly estimated that PI (Fig. 4 *d*) is oriented in a direction perpendicular to the DNA double strands ($\Psi \sim 90°$), whereas Hoechst (Fig. 4 *f*) is rather parallel to the DNA molecule ($\Psi \sim 0°$). It should be noted that the orientation of the samples corresponds to the neutral axis

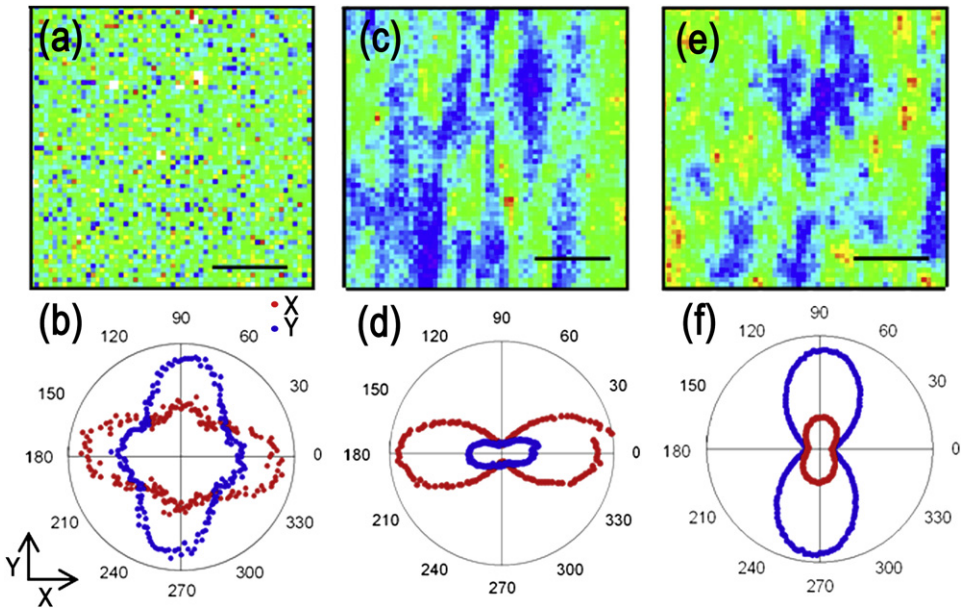


FIGURE 4 Nonlinear imaging and polarimetry measurements of isotropic and ordered DNA samples (60 mg/ml) labeled by PI and Hoechst. (*a* and *b*) Two-photon fluorescence intensity raster scan (*a*) and polar graph (*b*) representing *x* and *y* polarization components of DNA labeled by PI in isotropic solution. (*c* and *d*) Two-photon fluorescence intensity raster scan (*c*) and polar graph (*d*) of DNA labeled by PI in the liquid-crystalline phase. The orientation of DNA strands is $\phi = 90°$. (*e* and *f*) Two-photon fluorescence intensity raster scan (*e*) and polar graph (*f*) of DNA labeled by Hoechst liquid-crystalline phase. The orientation of DNA strands is $\phi = 90°$.

of the DM, and thus is not affected by possible depolarizing effects of the reflection.

To refine the analysis of the orientation of dye molecules bound to DNA, and to verify the conical distribution model for dye binding ($\Psi$ and $\Delta\Psi$), the samples were rotated in the *xy* plane to an arbitrary angle, $\phi$. In these conditions, the polarization of the incident linearly polarized light at the entrance to the microscope is modified by the DM before reaching the sample (23). A more detailed analysis of these effects is presented in Appendix 1.

Fig. 5 represents the polar graphs of PI- and Hoechst-emitted two-photon fluorescence intensity at different sample orientations, $\phi$. The direction of the lobes changes upon rotation of the DNA strands in the *xy* framework, which confirms that the orientation of the dyes is related to the direction of the DNA strands. The comparison between the experimental and theoretical graphs provides the binding angle $\Psi$. Considering that the emission dipoles of both fluorophores are within the plane of the molecule, the adjusted values are $\Psi = 80°$ ($\Delta\Psi = 10°$) and $\Psi = 20°$ ($\Delta\Psi = 10°$) for PI and Hoechst, respectively. This is compatible with the intercalation for PI and minor groove binding for Hoechst. The $\Psi$ value is in agreement with the binding parameters of PI determined by electrofluorescence spectroscopy (17,18). The binding angle of Hoechst is smaller than that determined by molecular modeling and electrofluorescence spectroscopy, ~35–40° (17,18), which may be due to the bias related to the existence of an angle between the absorption and emission dipoles. However, our data confirm the results of a fluorescence anisotropy study of Hoechst binding to DNA films, where the angle between the emission dipole and the DNA axis was found to be 170° (24).

The main advantage of nonlinear excitation is that it makes possible local analysis of the DNA orientation at a specific point on the sample. As shown in Fig. 3, *c* and *d*, the liquid-crystalline phases formed upon a drying process contain domains with different DNA orientations. Fig. 6 shows a two-photon fluorescence scan of a frontier region between two different domains. Since the polarization of the incident light is horizontal, the intensity of the emitted fluorescence gives a first insight into the PI orientation. The lower zone (*A*) of Fig. 6 *a* is much brighter than the upper zone (*B*), which indicates that PI molecules are aligned close to the horizontal direction in zone A and more vertically in zone B. In Fig. 6 *b*, the two-photon fluorescence intensity in the lower and upper zones (*C* and *D*) is almost identical,

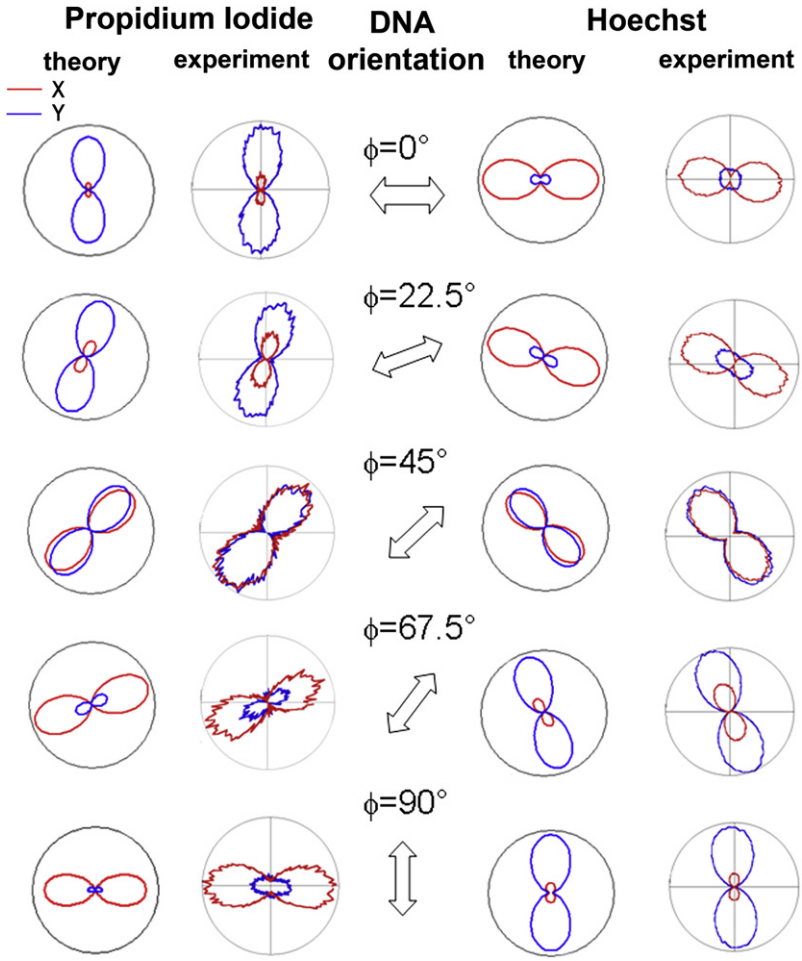


FIGURE 5 Polarimetric analysis of two-photon fluorescence of DNA-bound PI ($\lambda_{exc} = 920$ nm, $P = 1$ mW) and Hoechst ($\lambda_{exc} = 810$ nm, $P = 0.1$ mW). The double arrows represent the orientation of DNA strands ($\phi$). For each dye, the polar graphs in the first column correspond to simulated data and those in the second column to experimental data. Values for $\Psi$ and $\Delta\Psi$ parameters are $\Psi = 80°$, $\Delta\Psi = 10°$ for PI and $\Psi = 20°$, $\Delta\Psi = 10°$ for Hoechst.

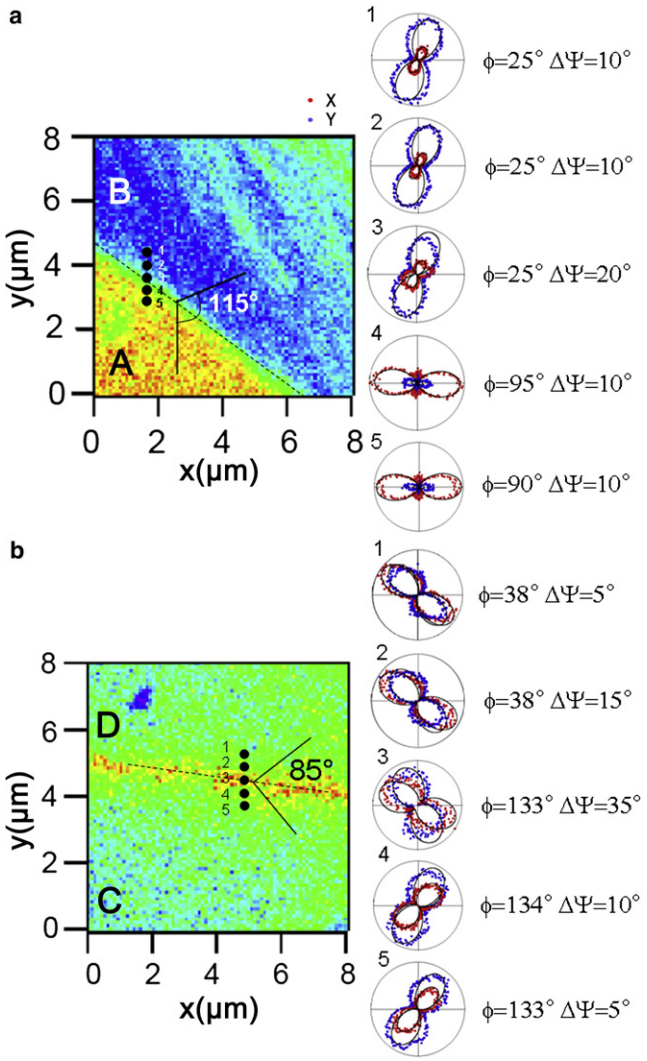


FIGURE 6 Two-photon fluorescence intensity raster scan of the border region between two LC domains of the characteristic zig-zag pattern at the perimeter of the dried DNA drop. The incident light is horizontally polarized. Polar graphs are measured in different points across the border line. (*a*) $\phi = 90^\circ$ and $\phi = 25^\circ$ for the lower (A) and upper (B) parts of the scan. (*b*) $\phi = 130^\circ$ and $\phi = 38^\circ$ for the lower (C) and upper (D) parts of the scan.

which means that the DNA strand orientation $-\phi$ should be symmetrical with respect to the border line. Two-photon polarimetric measurements were performed at different points across the contact line. The orientation of the DNA strands is almost constant within one domain but changes drastically after passing through the border line. A larger orientation distribution, $\Delta\Psi$, can be measured in the border region which means that the ordering is perturbed and entropy increases close to domain walls. The adjustment of the theoretical predictions to the experimental polar graphs revealed $\phi = 90^\circ$ and $\phi = 25^\circ$ for zones A and B, respectively, and $\phi = 133^\circ$ and $\phi = 38^\circ$ for zones C and D, respectively. Thus, the angle between the DNA strands in these domains is 115° in Fig. 6 *a* and 85° in Fig. 6 *b*. The relative orientations of the domains are symmetric with respect to the border line. In this way, by analyzing different points of the sample, it is possible to draw a DNA orientation map with lateral resolution currently down to 350 nm.

An important advantage of the nonlinear excitation is its intrinsic 3D sectioning capability, which enables analysis in all three dimensions. Fig. 7 shows two-photon fluorescence intensity raster scans and the associated polar graphs performed in different $z$ layers of a PI-labeled DNA LC closed cell. As can clearly be seen in the scans, in the proximity of the bottom coverglass the alignment of DNA strands is significantly different from that in the volume of the sample. The scan at $z = 0.5$ $\mu$m does not show any well defined structures, whereas the scans at $z = 3.0$ $\mu$m and $z = 15$ $\mu$m present some degree of organization. The $yz$ scan also shows a structured texture, even though its intensity decreases in the deeper regions because of the light scattering. The polar graphs were measured at different $z$-positions for the same $x$ and $y$ coordinates. The axial resolution of the microscope, as imposed by the diffraction limit is of the order of 0.8 $\mu$m. The polar graphs, measured by

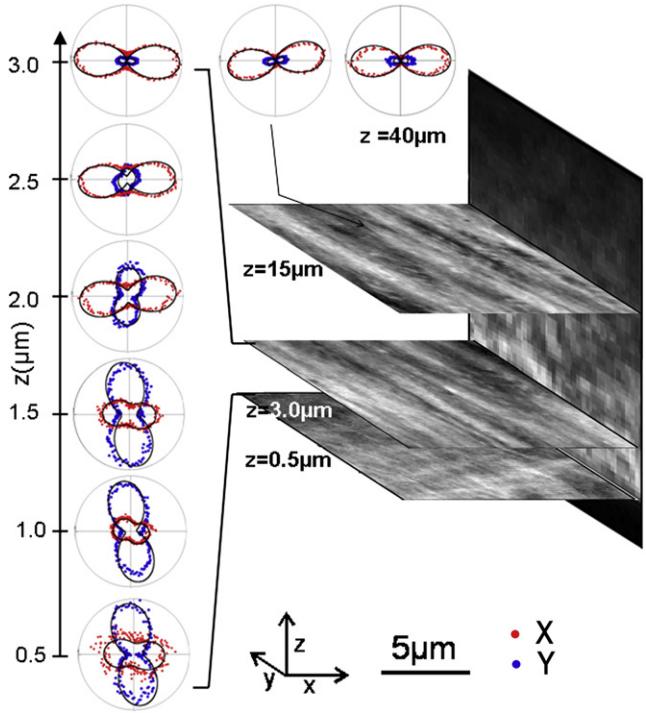


FIGURE 7 Two-photon fluorescence intensity raster scans in different depths of the DNA-LC closed cell along the $z$ axis of the microscope. $xy$ raster scans at different $z$ positions (0.5, 3.0, and 15 $\mu$m). Polar plots measured with fixed $x$ and $y$ coordinated at different $z$ positions were fitted with parameters as follows: $z = 0.5$ $\mu$m ($\phi = 165^\circ$, $\Psi = 75^\circ$, $\Delta\Psi = 15^\circ$, 17% isotropic); $z = 1.0$ $\mu$m ($\phi = 165^\circ$, $\Psi = 75^\circ$, $\Delta\Psi = 15^\circ$, 6% isotropic); $z = 1.5$ $\mu$m ($\phi = 165^\circ$, $\Psi = 75^\circ$, $\Delta\Psi = 15^\circ$, 10% isotropic); $z = 2.0$ $\mu$m ($\phi = 80^\circ$, $\Psi = 75^\circ$, $\Delta\Psi = 15^\circ$, 17% isotropic); $z = 2.5$ $\mu$m ($\phi = 85^\circ$, $\Psi = 80^\circ$, $\Delta\Psi = 15^\circ$, +4% isotropic); $z = 3.0$ $\mu$m($\phi = 80^\circ$, $\Psi = 80^\circ$, $\Delta\Psi = 15^\circ$); $z = 15$ $\mu$m ($\phi = 95^\circ$, $\Psi = 80^\circ$, $\Delta\Psi = 15^\circ$); and $z = 40$ $\mu$m ($\phi = 90^\circ$,$\Psi = 80^\circ$, $\Delta\Psi = 15^\circ$).

steps of 0.5 $\mu$m show important modifications, although the focal regions are superimposed. The orientation and shape of the lobes vary significantly over the first 3-$\mu$m-thick layers of the sample and then remain constant. This reorientation is probably due to interactions at the DNA/glass interface. The electrostatic interaction between the negatively charged DNA molecules and the glass surface might favor a different orientation from that imposed by the drying process, which becomes predominant further into the bulk of sample. These effects can be compared to anchoring effects, which are well documented but complex phenomena in liquid crystals (25). Similar effects were observed for DNA nematic dehydrated sheared films (26). However, in our case, the glass surface was not submitted to rubbing or related surface preprocessing that would have favored reorientation effects. Anchoring effects depend on factors such as the structure of the molecules, sample thickness, surface treatment, and interfacial properties (27,28). In our samples these effects also induce partial realignment and a subsequent loss of orientation of DNA molecules. To reach a better agreement with experimental data, an isotropic component of the DNA strand distribution has been introduced. Its relative proportion represents 17% at 0.5 $\mu$m from the glass surface and vanishes in the deeper regions.

It should be noted that polar graphs clearly point out the orientation of the dyes in deep regions of the samples (40 $\mu$m) also, even when the two-photon fluorescence intensity is low.

## DISCUSSION AND CONCLUSIONS

In this work, we have presented a polarization sensitive nonlinear microscopy study of the orientation of DNA in organized liquid-crystalline domains. The polarimetric analysis of two-photon fluorescence emitted by DNA-bound dyes shows that this technique is suitable for analyzing the orientation of molecules that associate in a specific way with DNA. The satisfactory correlation of the experimental results with our theoretical modeling makes it possible to distinguish between different DNA binding modes (intercalators or groove binding molecules). Working with fluorophores with well-known binding modes, this technique can be applied to study specific molecular arrangements of other types of LC phases and to realize a polarimetric map of the sample with high lateral and axial resolution.

The experimental data fit well with theoretical predictions, but some discrepancies remain, calling for the adjustment of the relative maximum intensity of $x$ and $y$ polarization components of the emitted fluorescence. The theoretical model is based on the assumption that all dipoles follow the same conical distribution. However, some depolarizing effects responsible for increasing the isotropic fluorescence background may occur due to partial disorder related to the nature of the samples. First, DNA molecules are not perfectly straight. The persistence length of a DNA molecule is of the order of 50 nm, leading to, on average, seven persistence lengths within a 350-nm focal spot of the microscope. Consequently, the emission dipoles are not perfectly aligned in the focus and the emitted fluorescence is partially depolarized. Second, in our experimental conditions, isotropic or amorphous domains coexist with organized ones, leading to the introduction of an isotropic component.

It should be noted that working with light-sensitive dyes raises the issue of light-induced effects. Measurements performed at different sample orientation in the $xy$ plane ($\phi$) show that the orientation of the dye follows the rotation of the sample and, thus, that the binding of the dye to the DNA strand is not disturbed by eventual light-induced forces related to irradiation.

These results show that the nonlinear polarimetry technique can be interesting for studying structural phase transition processes or coexistence of isotropic and anisotropic domains. Obviously, various experimental techniques are used to visualize the structure of liquid-crystalline phases. Most of these techniques provide only 2D information and are invasive to the sample to access the axial dimension (8,10,22). Scanning microscopy techniques are the best compromise toward 3D resolution, as they preserve the integrity of the sample. Z-sectioning can be achieved by rejecting the light from the out-of-focus planes by adding a pinhole to the excitation and detection optical path (confocal setup). Fluorescence confocal polarizing microscopy (FCPM) was successfully applied to the study of liquid crystals (11,22). Using this technique, the orientation of the emitting dipoles is derived from the fluorescence intensity measurement at fixed analyzer and polarizer orientations. However, the intensity-orientation relationship is conditioned by the homogeneity of the dye and DNA concentration (11). To make the measurement independent of the eventual concentration gradient of the dye or DNA, in this work, the polarimetry measurements are achieved locally by rotating the incident polarization angle by 360° at a given position within the sample. Besides this possibility of analysis of heterogeneous samples, a polarization analysis makes possible the precise determination of $\Psi$, $\Delta\Psi$, and $\phi$. Indeed, 3D sectioning is intrinsic to the excitation process, which requires a high concentration of incident photons and thus occurs exclusively at the focal spot. The advantage of nonlinear excitation is the significantly lower level of photobleaching of out-of-focus molecules and a deeper penetration of the excitation light into the sample. We note, therefore, that the nature of the information provided by FCPM and two-photon polarimetry is complementary. Assuming fixed and well determined dye binding to the host molecule, FCPM provides global information about the orientation of the director that is the average orientation of DNA chains. In contrast, two-photon polarimetry allows us to study locally and with high angular precision the position of the dye relative to the DNA strand and/or the orientation distribution of DNA molecules.

It should be mentioned, however, that DNA-dye interactions may influence the generation of liquid-crystalline phases compared to pure DNA (29). Indeed, intercalating dyes might significantly increase the length of DNA chains and the twist of the molecule, and thus perturb the organization of LC domains. Studies of doped DNA solutions reveal that the values of DNA concentration related to phase transition parameters are shifted, and that additional liquid-crystalline structures may also appear (21). Consequently the concentration of the dye should be kept at the lowest possible level compatible with the detection threshold to minimize the perturbation of the DNA structure.

Finally, the quality of the $z$-sectioning investigations depends on the conservation of the light beam features when traversing the sample. Scattering, defocusing effects, and modifications of the polarization of the incident light are minimal provided $(\Delta n^* z)/\lambda$ (where $\Delta n$ is the birefringence of the sample) is less than unity. Two-photon excitation that uses the infrared light thus offers a considerable advantage compared to single-photon microscopy.

The spatial resolution limit of two-photon microscopy (~350 nm) is sufficient at the scale of DNA liquid-crystalline domains, which have a size of a few micrometers. Applications to the field of biology are also of interest, since it has been proposed that the process of self-organization driven by noncovalent binding plays an important role in ordering of DNA and chromatin structures. The ordered structure is the best compromise for packing a maximum DNA length into a minimum volume, and the liquid properties are essential for the flexibility and accessibility of the regulation and transcription enzymes. Hence, liquid crystals are a plausible hypothesis of the natural organization of DNA (2,7,30).

Atomic force microscopy measurements show that sperm DNA packaged by protamines adopts a toroidal structure containing up to 60 kbp of DNA (31). Electron micrographs and circular dichroism studies of dinoflagellate

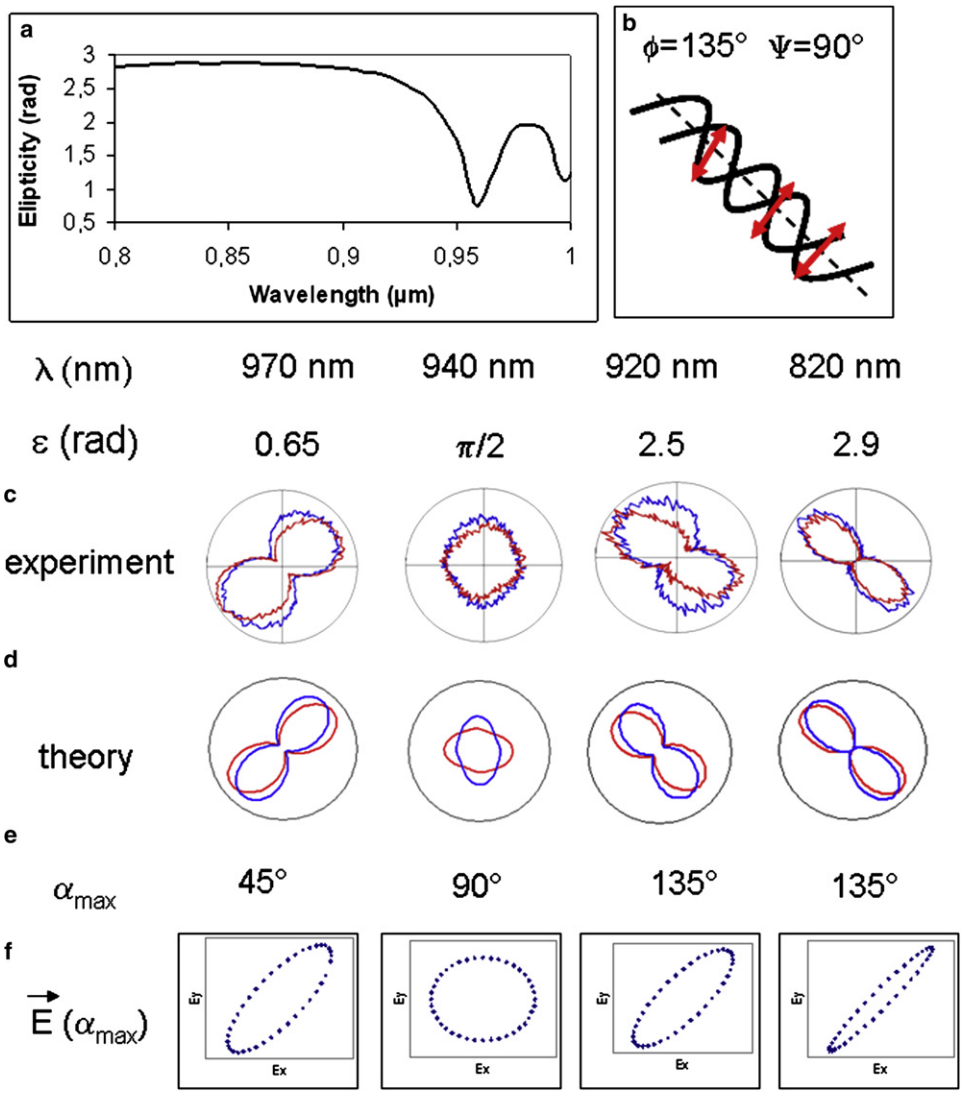


FIGURE 8 Ellipsometric measurements of the DM at the incident angle of 45° and its influence on fluorescence intensity. (*a*) Wavelength dependence of ellipticity $\varepsilon(\lambda)$. (*b*) Scheme of the DNA double-strand labeled by the PI (intercalator). (*c–f*) Polar graphs representing the intensities of the $x$ and $y$ polarization components of the two-photon fluorescence emitted. Experimental results (*c*) are measured with PI-labeled DNA, with the orientation of DNA domains at 135. The theoretical graphs (*d*) are calculated with $\Psi = 80°$, $\Delta\Psi = 10°$, and $\phi = 135°$ (see Fig. 1). The angle of maximum fluorescence intensity, $\alpha_{max}$ (*e*), changes with the excitation wavelength, but the direction of polarization of the electric field impinging on the sample at this angle, $\vec{E}(\alpha_{max})$ (*f*), remains the same, giving the polarization state.

chromosomes present a characteristic pattern for a cholesteric LC phase (32–34). X-ray scattering from bacteria with high-copy-number plasmids has also revealed the presence of cholesteric phases (30). These works suggest that DNA liquid-crystalline phases represent an efficient way of packaging high-copy-number plasmids (6). Moreover, it has been reported that due to specific geometric arrangements and secondary structures, DNA liquid crystals influence the regulation of intermolecular interactions of structures such as nucleosomes (2). The presence of liquid-crystalline domains has been described in nucleosome particle solutions (5,35), which indicates that they may play an important role in formation of nucleoprotein complexes. The work of Livolant et al. (20) has shown that because of the strong negative charge on the nucleosome surface due to the DNA molecule, the transitions between columnar isotropic, lamellocolumnar, and columnar hexagonal phases are driven by the ionic strength of the solution and the applied pressure. Even if the correspondence between these models and the real chromatin higher-order structures is not fully clarified, these works provide a library of possible structures for chromatin organization in vivo (2); for instance, it has been proposed that telomeric chromatin is organized in a columnar phase (36).

Finally, to allow a detailed examination of tiny structures such as 30-nm nucleosome fibers or the chromatin topology in the nucleus, resolution should be further increased by use of subdiffraction microscopy techniques. The increase of the resolution to nanoscopic scale (37) would promote nonlinear polarimetry as a relevant tool for inferring DNA organization in physiological structures.

## APPENDIX A

To analyze the polar graphs, it should be noted that the variable angle $\alpha$ corresponds to the polarization angle of the incident light before the reflection by the DM, whereas the angle of maximum fluorescence intensity, $\alpha_{max}$, depends on the orientation of the sample molecules and the polarization of the light impinging on the sample after the DM reflection. The depolarizing effects of the DM, such as the ellipticity, $\varepsilon$, and relative reflectivity, $\delta$, for $s$ and $p$ polarization components should thus be taken into account (23). As measured by ellipsometry, the $\delta$ value is ~1.02 and can be considered constant throughout the wavelength range. On the contrary, the ellipticity, $\varepsilon$, shows important variations in the spectral region between 900 and 1000 nm (Fig. 8 *a*). The consequences of such modifications are illustrated by polar graphs corresponding to constant DNA orientation ($\phi = 135°$) (Fig. 8 *b*), but at different excitation wavelengths ($\lambda = 970$ nm, 940 nm, 920 nm, and 820 nm). The experimental data are measured with PI-labeled DNA that forms LC phases in a closed-cell environment. All experimental parameters are kept constant with the exception of the excitation wavelength. As shown in Fig. 8 *c*, the orientation and the form of the $x$ and $y$ intensity components vary in an important way. These experimental results are compared to simulated curves with the parameters $\Psi = 90°$, $\Delta\Psi = 5°$, $\phi = 135°$, and with different $\varepsilon$ values equal 0.65, $\pi/2$, 2.5, and 2.9 rad, corresponding to the DM-induced ellipticity, $\varepsilon$, at the selected wavelengths (Fig. 8 *d*). The corresponding graphs are in good agreement with experiments. The angle of maximum emission in the polar graphs, $\alpha_{max}$ (Fig. 8 *e*), is dependent on the average orientation of the emission dipoles and on $\varepsilon$. Since we consider a sample with PI molecules oriented at ~45°, the polarization impinging on the sample at $\alpha_{max}$ is set at a fixed orientation (Fig. 8 *f*). The direction equals 45° in all graphs.

This example shows that considering both the orientation and the shape of the lobes, the analysis of polar patterns is strongly dependent on the $\varepsilon$ value and thus on the choice of excitation wavelength. Overlooking the anisotropies of the DM can clearly lead to important errors in the interpretation of polarimetric data.

Taking into account the DM ellipticity, the excitation wavelengths used in the experiments for PI and Hoechst were 920 nm and 810 nm, with ellipticity values $\varepsilon = 2.5$ rad and $\varepsilon = 2.8$ rad, respectively.

We are grateful to Prof. J.-F. Mouscadet and Dr. S. Bury-Moné for their constructive comments concerning DNA structure and topology. We thank Dr. Thanh Nguyen for the ellipsometry measurements of the dichroic mirror, and Dr. Sophie Brasselet and Dr.Véronique Le Floc'h for previous works on the nonlinear microscope setup.

This work was supported by grants from the French National Resource Agency (ANR Imfovir PCV-2006) and from Région Ile-de-France, and by the European Commission through the Human Potential Programme (Marie-Curie RTN BIMORE, MRTN-CT-2006-035859 and N50713231/3302).

## REFERENCES

1. Zakharova, S. S., W. Jesse, C. Backendorf, and J. R. van der Maarel. 2002. Liquid crystal formation in supercoiled DNA solutions. *Biophys. J.* 83:1119–1129.
2. Livolant, F., S. Mangenot, A. Leforestier, A. Berlin, M. Frutos, et al. 2006. Are liquid crystalline properties of nucleosomes involved in chromosome structure and dynamics? *Philos. Transact. A Math. Phys. Eng. Sci. 2615–2633*.
3. Fraden, S., and R. D. Kamien. 2000. Self-assembly in vivo. *Biophys. J.* 78:2189–2190.
4. Strzelecka, T. E., M. W. Davidson, and R. L. Rill. 1988. Multiple liquid crystal phases of DNA at high concentrations. *Nature.* 331: 457–460.
5. Leforestier, A., and F. Livolant. 1997. Liquid crystalline ordering of nucleosome core particles under macromolecular crowding conditions: evidence for a discotic columnar hexagonal phase. *Biophys. J.* 73:1771–1776.
6. Reich, Z., E. J. Wachtel, and A. Minsky. 1994. Liquid-crystalline mesophases of plasmid DNA in bacteria. *Science.* 264:1460–1463.
7. Bloomfield, V. A. 1996. DNA condensation. *Curr. Opin. Struct. Biol.* 6:334–341.
8. Merchant, K., and R. L. Rill. 1997. DNA length and concentration dependencies of anisotropic phase transitions of DNA solutions. *Biophys. J.* 73:3154–3163.
9. Kassapidou, K., W. Jesse, J. A. van Dijk, and J. R. van der Maarel. 1998. Liquid crystal formation in DNA fragment solutions. *Biopolymers.* 46:31–37.
10. Morii, N., G. Kido, H. Suzuki, and H. Morii. 2005. Annular self-assembly of DNA molecular chains occurring in natural dry process of diluted solutions. *Biopolymers.* 77:163–172.
11. Smalyukh, I., S. V. Shiyanovskii, and O. D. Lavrentovich. 2001. Three-dimensional imaging of orientational order by fluorescence confocal polarizing microscopy. *Chem. Phys. Lett.* 336:88–96.
12. Denk, W., J. H. Strickler, and W. W. Webb. 1990. Two-photon laser scanning fluorescence microscopy. *Science.* 248:73–76.
13. Le Floc'h, V., S. Brasselet, J. F. Roch, and J. Zyss. 2003. Monitoring of orientation in molecular ensembles by polarization sensitive nonlinear microscopy. *J. Phys. Chem. B.* 107:12403–12410.
14. Brasselet, S., V. LeFloc'h, F. Treussart, J. F. Roch, and J. Zyss. 2004. In situ diagnostics of the crystalline nature of single organic nanocrystals by nonlinear microscopy. *Phys. Rev. Lett.* 92:2074701.
15. Brasselet, S., and J. Zyss. 2007. Nonlinear polarimetry of molecular crystals down to the nanoscale. *C.R. Phys.* 8:165–179.

16. Le Xuan, L., Ch. Zhou, A. Slablab, D. Chauvat, C. Tard, et al. 2007. Photostable single KTiOPO4 nanocrystals for second-harmonic generation microscopy. *Proc. IEEE/LEOS Internatl. Conf. Opt. MEMS Nanophotonics*. 39–40.

17. Pjura, P. E., K. Grzeskowiak, and R. E. Dickerson. 1987. Binding of Hoechst-33258 to the minor groove of B-DNA. *J. Mol. Biol.* 197: 257–271.

18. Windsor, S. A., and M. H. Tinker. 1996. Binding of biologically important molecules to DNA, probed using electro-fluorescence polarization spectroscopy. *Biophys. Chem.* 58:141–150.

19. Le Floc'h, V., S. Brasselet, J. Zyss, B. R. Cho, S. H. Lee, et al. 2005. High efficiency and quadratic nonlinear optical properties of a fully optimized 2D octupolar crystal characterized by nonlinear microscopy. *Adv. Mater.* 17:196–200.

20. Livolant, F., and A. Leforestier. 1996. Condensed phases of DNA: structures and phase transitions. *Prog. Polym. Sci.* 21:1115–1164.

21. Olesiak, J., K. Matczyszyn, H. Mojzisova, M. Zielinski, D. Chauvat, et al. 2009. Liquid crystalline phases in DNA and DNA-doped soutions analysed by polarized linear and nonlinear microscopy and differential scanning calorimetry. *Mater. Sci. Poland.* In press.

22. Smalyukh, I. I., O. V. Zribi, J. C. Butler, O. D. Lavrentovich, and G. C. Wong. 2006. Structure and dynamics of liquid crystalline pattern formation in drying droplets of DNA. *Phys. Rev. Lett.* 96: 177–801.

23. Schon, P., F. Munhoz, A. Gasecka, S. Brustlein, and S. Brasselet. 2008. Polarization distortion effects in polarimetric two-photon microscopy. *Opt. Express*. 16:20891–20901.

24. Morii, N., G. Kido, T. Konakahara, H. Morii, et al. 2005. Orientation of dye molecules in DNA-based films with chain alignment and judgment of their DNA-binding modes. *J. Phys. Chem. B*. 109:15636–15644.

25. Jerome, B. 1991. Surface effects and anchoring in liquid crystals. *Rep. Prog. Phys.* 54:391–451.

26. Nakata, M., G. Zanchetta, M. Buscaglia, T. Bellini, N. A. Clark, et al. 2008. Liquid crystal alignment on a chiral surface: interfacial interaction with sheared DNA films. *Langmuir*. 24:10390–10394.

27. Bonvent, J. J., I. H. Becgtold, M. L. Vega, E. A. Oliveira, et al. 2000. Alignment and phase transition induced by surface action in lyotropic nematic liquid crystals. *Phys. Rev. E Stat. Phys. Plasmas Fluids Relat. Interdiscip. Topics.* 62:3775–3779.

28. Guyotsionnest, P., H. Hsiung, and Y. R. Shen. 1986. Surface polar ordering in a liquid crystal observed by optical second-harmonic generation. *Phys. Rev. Lett.* 57:2963–2966.

29. Lerman, L. S. 1961. Structural considerations in interaction of DNA and acridines. *J. Mol. Biol.* 3:18–30.

30. Reich, Z., S. Levin-Zaidman, S. B. Gutman, T. Arad, and A. Minsky. 1994. Supercoiling-regulated liquid-crystalline packaging of topologically-constrained, nucleosome-free DNA molecules. *Biochemistry.* 33:14177–14184.

31. Hud, N. V., M. J. Allen, K. H. Downing, J. Lee, and R. Balhorn. 1993. Identification of the elemental packing unit of DNA in mammalian sperm cells by atomic force microscopy. *Biochem. Biophys. Res. Commun.* 193:1347–1354.

32. Rill, R. L., F. Livolant, H. C. Aldrich, and M. W. Davidson. 1989. Electron microscopy of liquid crystalline DNA: direct evidence for cholesteric-like organization of DNA in dinoflagellate chromosomes. *Chromosoma*. 98:280–286.

33. Livolant, F., and Y. Bouligand. 1978. New observations on twisted arrangement of dinoflagellate chromosomes. *Chromosoma.* 68:21–44.

34. Bouligand, Y., and V. Norris. 2001. Chromosome separation and segregation in dinoflagellates and bacteria may depend on liquid crystalline states. *Biochimie*. 83:187–192.

35. Mangenot, S., A. Leforestier, D. Durand, and F. Livolant. 2003. Phase diagram of nucleosome core particles. *J. Mol. Biol.* 333:907–916.

36. Fajkus, J., and E. N. Trifonov. 2001. Columnar packing of telomeric nucleosomes. *Biochem. Biophys. Res. Commun.* 280:961–963.

37. Hell, S. W. 2003. Toward fluorescence nanoscopy. *Nat. Biotechnol.* 21:1347–1355.